Design of organically modified sepiolite and its use as adsorbent for hazardous Malachite Green dye removal from water

Fadwa Largo, Redouane Haounati, Hassan Ouachtak, Naima Hafid, Amane Jada, Abdelaziz Ait Addi

Design of organically modified sepiolite and its use as adsorbent for hazardous malachite green dye removal from water

Fadwa LARGO[a], Redouane HAOUNATI[a], Hassan OUACHTAK[b, c], Naima HAFID[d], Amane JADA[e, f,*], Abdelaziz AIT ADDI[a]

[a] Physical Chemistry & Environment Team, Faculty of Sciences, Ibn Zohr University, Agadir, Morocco

[b] Department of Applied Chemistry, Faculty of Applied Sciences. Ibn Zohr University, Ait Melloul, Morocco

[c] Applied Chemistry & Environment Laboratory, Applied Bio-Organic Chemistry Team, Faculty of Sciences, Ibn Zohr University, Agadir, Morocco

[d] Center For Education & Training Profession Souss Massa, Morocco

[e] Institute of Materials Science of Mulhouse (IS2M), Haute Alsace University, Mulhouse 68100, France

[f] Strasbourg University, Strasbourg 67081, France

*Corresponding author: amane.jada@uha.fr ;

Abstract

A novel adsorbent design method, based on organic surface modification and carbonization at 350-500°C, of sepiolite, was used to prepare carbon@sepiolite composites which were used for hazardous malachite green dye removal from water. Prior to their use as adsorbent, the structure and the morphology of the carbon@sepiolite composites were assessed by various methods, such as, Fourier Transform Infra-Red (FTIR) spectroscopy, Scanning (SEM) and Transmission (TEM) Electron Microscopy, Energy Dispersive Analysis of X-rays (EDAX), and N_2 adsorption/desorption isotherms (BET method). The designed adsorbents showed good adsorption properties for MG molecules, reaching a maximum dye adsorbed amount of 1198.67 mg/g at 25°C for the carbon@sepiolite composites calcinated at 500°C. Further, the kinetics and the equilibrium adsorption isotherms of the MG molecules from water onto the sepiolite-based composites, were well fitted by, respectively, the pseudo-second-order model (R^2 =0.98) and the Langmuir isotherm (R^2= 0.94) models, indicating that the MG molecules were homogenously adsorbed and formed a monolayer on the organically modified sepiolite surface. Moreover, the values of the thermodynamic parameters, such as ΔG, ΔH and ΔS related to the adsorption process, indicated that the adsorption reaction was spontaneous, feasible and endothermic. In the overall, the present work offers facile ways for the design of organically modified sepiolite which can be used at large scale as adsorbents for waste recycling.

Keywords: Clay; Malachite Green dye; Sepiolite; Adsorption; Waste.

1. Introduction

Organic dyes are extensively worldwide used and mainly in industrial sectors, such as, in the pulp and paper industry, in the food and paint industries, also in the wool, cotton, leather, silk and textile industries[1, 2]. All these industries using organic dyes are generating colored wastewater, leading to a major and a serious environmental problem [3, 4]. Due to their persistent characteristics, their teratogenicity and carcinogenicity, the organic dyes are toxic to humans and to the environment [5–9]. Moreover, water polluted by dyes leads to many health problems such as allergic dermatitis, skin problems, and cancer in humans [10–12]. To treat the colored water and/or the contaminated water, various chemical, physical and biological methods, have been developed [13–15]. However, it is essential to develop efficient and inexpensive methods. Thus, the adsorption is one of the best and most competitive ways to treat wastewater, due to various advantages, such as, its easy handling, its high efficiency, its low cost and the wide availability of the adsorbent materials [16, 17]. Further, the adsorption process does not generate any secondary pollution[18]. On an other hand, when selecting the adsorbent we have to take into account the fact that the real textile effluents contain mixture of several dyes [6, 19]. Thus, in order to elucidate the dye adsorption mechanism from water onto the adsorbent, it is essential to consider initially single-dye systems to reduce the complexity occurring in the real textile effluent treatment. For this reason, various types of adsorbents have been extensively used to treat wastewaters, such as activated carbon [20]. However, due to the high costs of these adsorbents, researches have been carried out to find low-cost adsorbents having high surface areas, high sorption capacities, and having sustainable and regeneration capabilities. Different types of adsorbents such as sepiolite, montmorillonite organoclay composites [21], modified sepiolite [22], mesoporous silica [23] have been used for the removal of dyes from wastewater. It should be noted that sepiolite (Sep) is a 2:1 type clay mineral, with an excellent adsorption property due its large specific

surface area, its high porosity, its ion exchange capacity [3], and its typical structural properties and its low cost, make it useful in various fields as promising adsorbent for dye wastewater treatment. As well as, its high surface polarity making the sepiolite surface negatively charged, which is balanced by inorganic cations (e.g., Na^{+}, Ca^{2+}). These inorganic cations are exchangeable, making Sep efficient adsorbent for various cationic dyes. Proper disposal of the used Sep is critical to the wide application of Sep in dye wastewater treatment. However, desorption of cationic dyes from the used Sep can be very difficult, because of the strong electrostatic interaction between cationic dyes and Sep. As such, traditional regeneration methods based on desorption are not efficient for recovering the used Sep. Direct landfill disposal of the used Sep will not only cause serious environmental pollution, but also be a huge waste of Sep resources. For this reason, it is urgent to find proper methods to dispose the used Sep.

In the present work, MG was selected as a representative of cationic dyes, and after its adsorption to Sep, the resulting used Sep (MG–Sep) was collected and calcined at different temperatures, enhancing hence the disaggregation and the performance of the clay. Such synthesis method producing functional adsorbent is expected to provide a simple way for treating waste and recycling the organic clay minerals. Further, to improve the adsorptive and regeneration properties of the sepiolite, the aim of the present work is to decrease, on one hand, the sepiolite clay mineral surface high polarity, and to increase on the other hand, its channels and tunnels spacing. Such synthesis method producing functional adsorbent is expected to provide a simple way for treating waste and recycling the organic clay minerals.

The characteristics of the resultant materials (Carbon@Sep) were identified by using methods such as, FTIR, BET, SEM, TEM and EDS. This study aimed firstly to compare the differences in properties of the raw sepiolite, calcined sepiolite and the composite-produced from the carbonization method, and secondly to examine the performance of the

carbon@sepiolite in the MG dye removal. Thus, to examine the Carbon@Sep adsorptive affinity towards the cationic dye removal, experiments were realized by varying physicochemical conditions (initial pH, adsorbent dosage, MG dye concentration, adsorption time and temperature). In addition to the experimental adsorption data, theoretical modeling of the kinetic and the equilibrium dye adsorption on the prepared adsorbent, were also carried out.

2. Experimental

2.1. Materials

The sepiolite (Sep) used in this work was collected from Eskişehir region, in Turkey. It was crushed and sieved to the desired particle size of less than 50 µm. Malachite Green (MG, Mw: 364.91, purity ≥99.00%) was obtained from Sigma–Aldrich, and it was used without any further treatment. The characteristics of MG cationic dye are presented in Table 1 (please see the supplementary file). Aqueous dye solution was prepared by dissolving the required mass of the dye in bi-distilled water.

2.2. Preparation of the organic modified sepiolite

Organic Sep (OSep) was prepared by reconstructing Sep structure in MG solution. Thus, Sep was first dispersed in MG solution, 1 g of Sep was added into 1 L of 100 mg/L ($0.274.10^{-3}$ Mole/L) MG solution for 6 h. After MG adsorption from water onto Sep (MG adsorbed amount of 95.4 mg/g), the resulting used Sep (MG–Sep) was collected and calcined at different temperatures ranging from 350 to 500 °C for 3 hours, by using a temperature-controlled furnace. The resulting calcined (MG-Sep) composites were labeled as (Carbon@Sep).

3. Characterization methods

Surface morphologies of the samples were observed by using a Scanning Electron Microscope (SEM, Supra 40 VP Gemini Zeiss Column), with a maximum voltage of 20 KV.

Structural features of the samples were assessed by acquiring images thanks to Transmission electron microscopy (TEM, Philips, CM 200), operating at an acceleration voltage of 20-200 kV with a magnification ranging from ×10 000 to ×200 000.

The chemical composition and the elemental distribution of the samples were determined by Energy Dispersive X-ray Analysis (EDAX). The specific surface areas and the porosities of the samples were assessed by treating the experimental N_2 adsorption-desorption data, as performed at 77 K (Micrometrics instrument, ASAP2420), by BET and BJH methods, respectively.

4. Adsorption experiments

Experiments of MG dye removal by Carbon@Sep were conducted by using batch equilibrium technique. Thus, firstly 1 L of MG stock solution having a dye concentration of 1200 mg/L, was prepared by dissolving 1200 mg of the dye in 1 L of distilled water, and then other solutions of desired concentrations were obtained by successive dilution of this stock solution. Thus, various adsorbate-adsorbent mixture series having initial dye concentration of 100 mg/L were prepared by placing in each 100 ml glass flask, a volume (50 ml) of the diluted MG solution. Thereafter, various adsorbent amounts (0.2 - 1.5 g) were added to the 100 ml glass flasks and the mixtures were agitated.

In order to investigate the aqueous phase pH, the contact time and the temperature effects, the pH was varied in the range (2-10); the contact time covered the interval (5– 420 min), whereas the temperature ranged in the interval (298-333 K). Thus, various adsorbate-adsorbent mixture series having initial dye concentration of 100mg/L were prepared. Further, the pH values of dye aqueous solutions were adjusted by using 0.1 N hydrochloric acid and 0.1 N sodium hydroxide aqueous solutions. It should be noted that after each dye adsorption experiment, the resulted dispersion was filtered through 0.2 µm Millipore membrane filter, and the residual dye concentrations were analyzed at λ_{max}= 618 nm using UV-Visible

spectrophotometer (UV-1800, SHIMADZU). The adsorbed amount at the equilibrium (q_{ads}, mg g^{-1}), and the removal percentage (% R), of the MG dye were calculated by using, respectively, the following equations (1) and (2):

$$q_{ads} = \frac{C_0 - C_e}{m} xV \qquad \textbf{(Eq. 1)}$$

$$\%_{\text{Removal}} = \frac{C_0 - C_e}{C_0} \text{x}100 \qquad \textbf{(Eq. 2)}$$

where q_{ads} is the amount of the adsorbed dye (mg/g), C_0 and Ce are the initial and the equilibrium concentrations of the dye (mg/L), V (L) is the volume of solution and m (g) is the Carbon@Sep mass.

5. Results and discussion

5.1. Characterization

5.1.1. FTIR analysis

The FTIR Spectra of the all prepared samples were recorded from 400 cm^{-1} to 4000 cm^{-1} and they were comparatively investigated. As can be seen in Fig. 1, for the sepiolite, the FTIR spectrum shows all characteristic peaks of clay mineral. Thus, the 3584 and 1671 cm^{-1} bands are assigned, respectively, to the OH stretching, representing the zeolitic water in the channels, and to the bound water coordinated to magnesium in the octahedral sheet. The band occurring at 1405 cm^{-1} is due to the hydroxyl bending vibration, reflecting hence, the presence of bound water. The Si–O coordination bands occurring at 1213 and 1017 cm^{-1} represent the stretching of Si–O in the Si–O–Si groups of the tetrahedral sheet. When compared to the raw Sepiolite (Sep) spectrum, FTIR spectra of the modified sepiolite (carbon@Sep 450°C and carbon@Sep 500°C) show the appearance of all sepiolite bands. In

addition, significant decrease in the intensity of all bands were observed, which may be due to a greater decrease for Si^{4+} cations, as compared to Mg^{2+} cations caused by high temperature, changing hence the sepiolite surface structure.

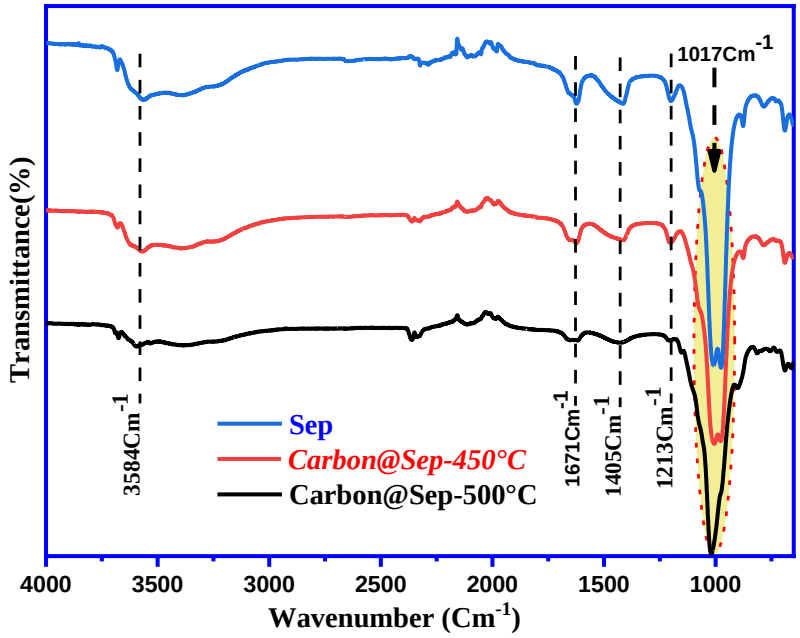

Fig. 1. FTIR Spectra of raw Sepiolite, Carbon@Sep-450°C, Carbon@Sep-500°C.

5.1.2. SEM and EDAX analyzes

The surface morphology and the composition of the calcined raw Sep and the carbon@sepiolite composites, were assessed by using SEM-EDAX instrument in order to get deeper information on the structural characteristics of the materials, as depicted in Fig. 2. In addition, the elemental composition data are presented in Table 2. Thus, as can be observed in Fig. (a) The sepiolite exists in the forms of lamellar particles, as well as, crystal bundles. When the original sepiolite, the organic and the calcined sepiolite, are compared, it is shown that the original morphology and the microstructure of the sepiolite crystals are kept intact after organic and thermal modifications. Further, as shown in Fig.2 c-e, after the organic and

184 the thermal modifications of the sepiolite, the original crystalline structure of the material was
185 maintained, and the fiber aggregation phenomenon of the sepiolite decreased more in the
186 modified sepiolite in comparison to the pristine one. Moreover, the carbonization process of
187 OSep at 500 °C, as depicted in Fig.2 (e), gives material having still large pore diameters and
188 more homogeneous surface. On the contrary, the raw sepiolite calcined at 500 °C, Fig. 2 (b),
189 shows a lower pore volume in comparison to the Carbon@Sep calcinated at 500 °C.

190 According to the elemental composition results (Table 2), the carbon element is evenly
191 distributed along with Silica, Magnesium and Oxygen elements in the Carbon@Sep
192 composite produced from the carbonization of the same precursor (Sep/MG) at temperatures
193 ranging from 400 °C to 500 °C. Note that during the carbonization process, the resulting
194 carbon mass percentage increases from 39 % to 49.7%, by going from 400 °C to 500 °C.
195 Further, the EDS data indicate uniform distribution of carbon nanoparticles in the
196 Carbon@Sep composites, and confirm the successful modification of sepiolite, by grafting the
197 C element in it.

198 **Table 2: Elements mass percentages of the raw Sep, calcined raw sepiolite at 500 °C,**
199 **Carbon @Sep(400 °C), Carbon@Sep(450 °C) and Carbon@Sep(500 °C)**

Sample	Si	Mg	O	C	Ca
Sepiolite	**37.8**	**17.6**	**44.6**	**--**	**--**
Raw Sep. calcined at 500 °C	**31.1**	**16.6**	**46.5**	**--**	**5.9**
Carbon@Sep (400 °C)	**12.5**	**8.5**	**39.6**	**39.2**	**0.3**
Carbon@Sep (450 °C)	**10.9**	**7.3**	**36**	**45**	**0.5**
Carbon@Sep (500 °C)	**8.8**	**6.3**	**34.5**	**49.7**	**0.3**

200

201 **5.1.3. TEM analysis**

202 The TEM images of the raw Sep, the raw Sep calcined at 500 °C, and Carbon@Sep
203 composites are shown in Fig.3.

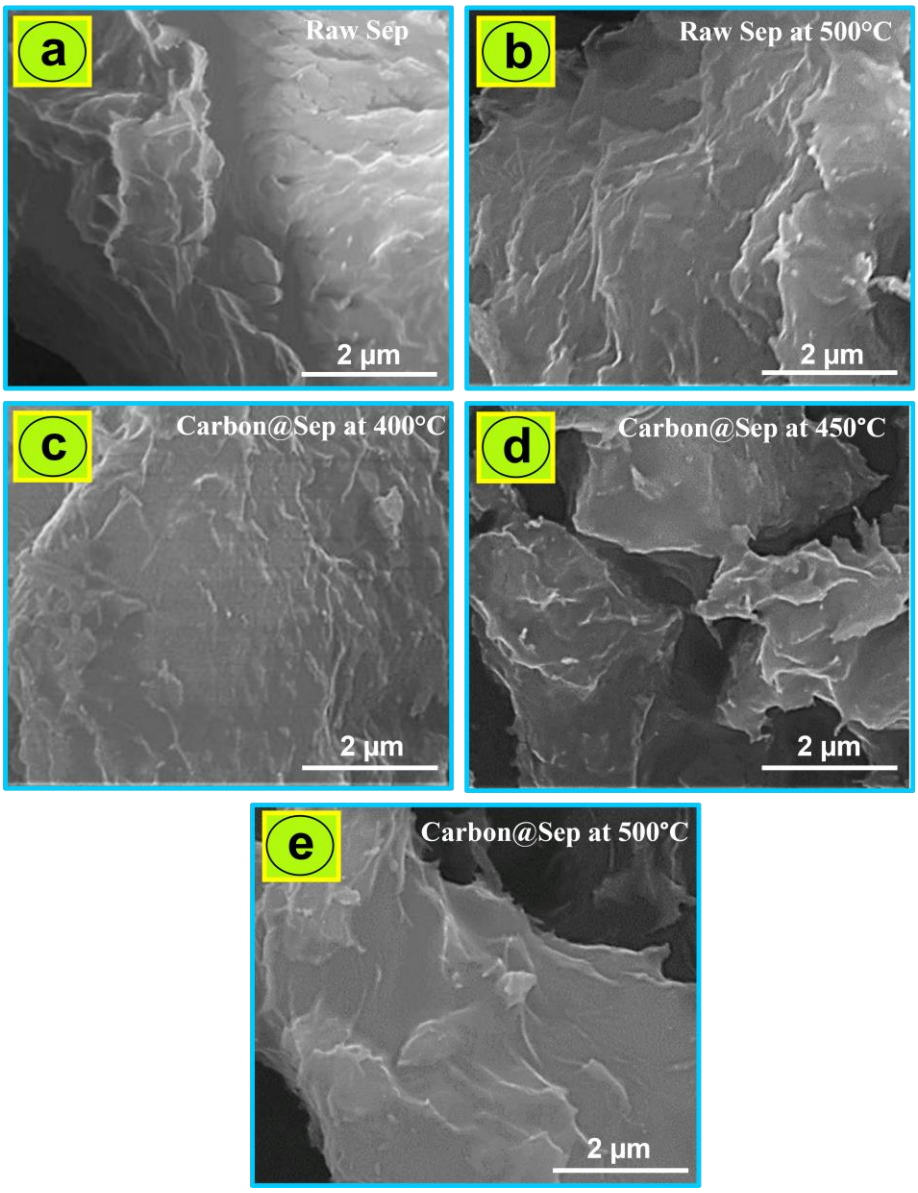

204

205 **Fig.2. SEM micrographs of raw sepiolite (a), raw sepiolite at 500 °C (b), Carbon@Sep at**
206 **400 °C (c), Carbon@Sep at 450 °C (d), Carbon@Sep at 500 °C (e).**

207 It can be seen in this figure that the raw Sep, and the Carbon@Sep resulted at different
208 temperature treatments, present all the needle-like fibrous clusters microstructure. space.
209 Furthermore, in Fig.3 (e), it can be observed larger bundles and disordered fibers structure.

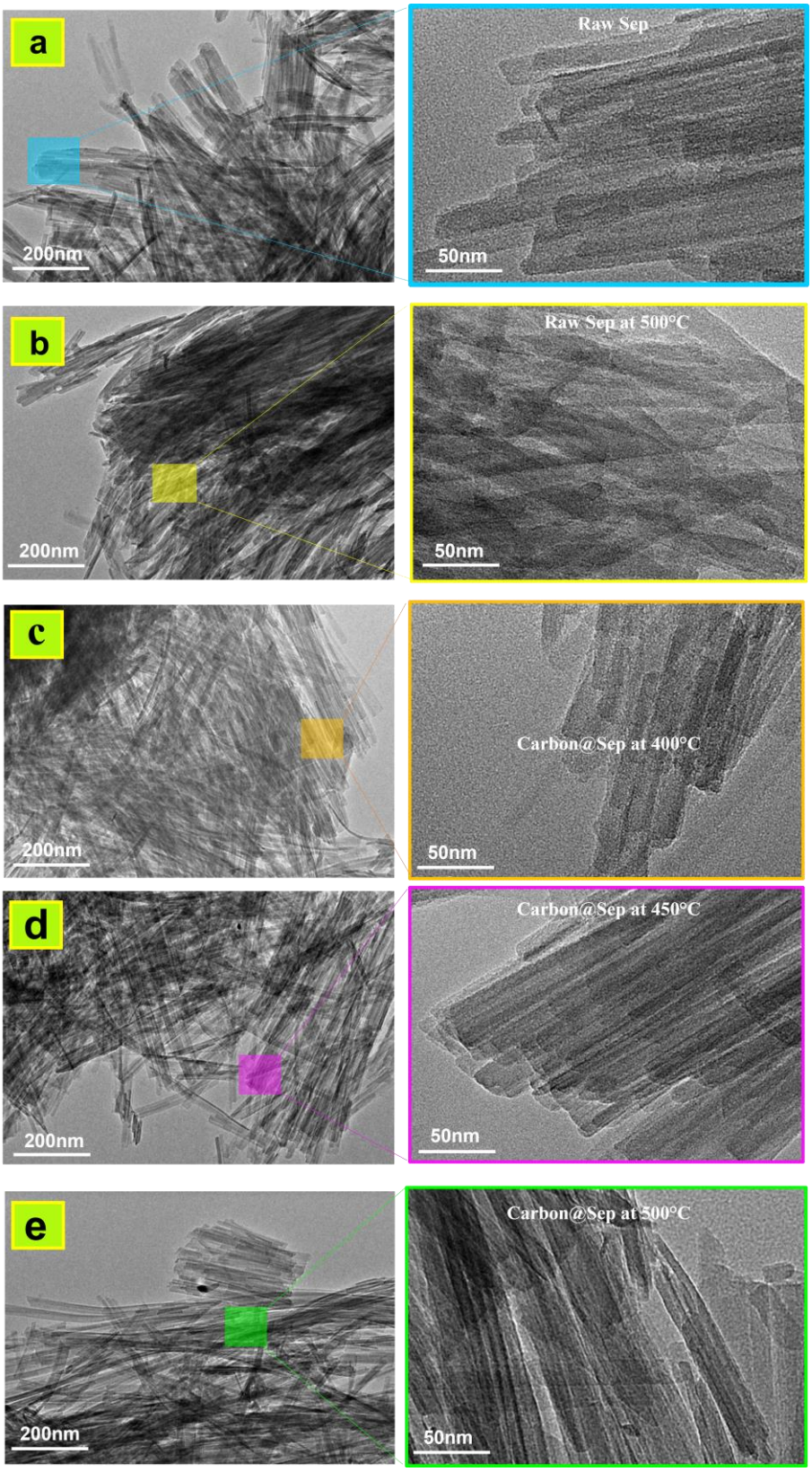

Fig.3. TEM images of the samples; all the samples present short micro-fibrous bundles like morphology

Further, it can be observed in Fig.3 (b) that the calcined raw Sep at 500 °C gives low inter fibrous bundles distance. On the other hand, Fig.3 (c, d) show a more developed inter-fibrous bundles

5.1.4. BET surface area assessment

The N_2 adsorption/desorption isotherms and the Barrett-Joyner-Halenda (BJH) pore size distributions of the five samples are illustrated in Fig.4., the calculated BET surface areas, pore volumes, and pore sizes, are presented in Table 3. Fig.4 indicates for all samples, that the N_2 adsorption-desorption isotherms are of type IV with hysteresis loops, mostly attributed to mesoporous materials, according to IUPAC classification. From these isotherms, the calculated specific surface area and the pore volume of the Sep were found to be, respectively, 300 m^2/g and 0.443 cm^3/g. However, after the successive carbonization of the carbon@Sep composite in the temperature range 400-500 °C, the specific surface area was found to decrease from 300.7 m^2/g for the raw Sepiolite, to 202.4 m^2/g and 149.48 m^2/g, for the Sep/MG composites treated at 400 °C and at 450 °C, respectively. Such decrease in the clay surface area indicates that N_2 molecules are not easily accessible to the calcined carbon@Sep sepiolite channels, which is filled by the carbon molecules. On the other hand, the comparison of the carbon@Sep samples carbonized, at 450 °C and 500°C, show increases in the specific surface area, and in the pore volume, from 149.8 to 207.5 m^2/g, and from 0.371 to 0.476 cm^3/g, respectively. Such results suggest that the carbonized sample (carbon@Sep composite at 500 °C) has an open structure, which is suitable to promote the penetration of the adsorbed molecules inside the composite surface. In addition, the average pore diameters of the raw Sep, the raw Sep calcined at 500 °C, the Carbon@Sep at 400 °C, 450 °C and 500 °C samples were calculated by using the BJH method, and they were found to be equal to, respectively, 37,78 Å, 38.34Å, 38.19Å, 38.18 Å and 38.26Å. Hence from these data, we can say that the

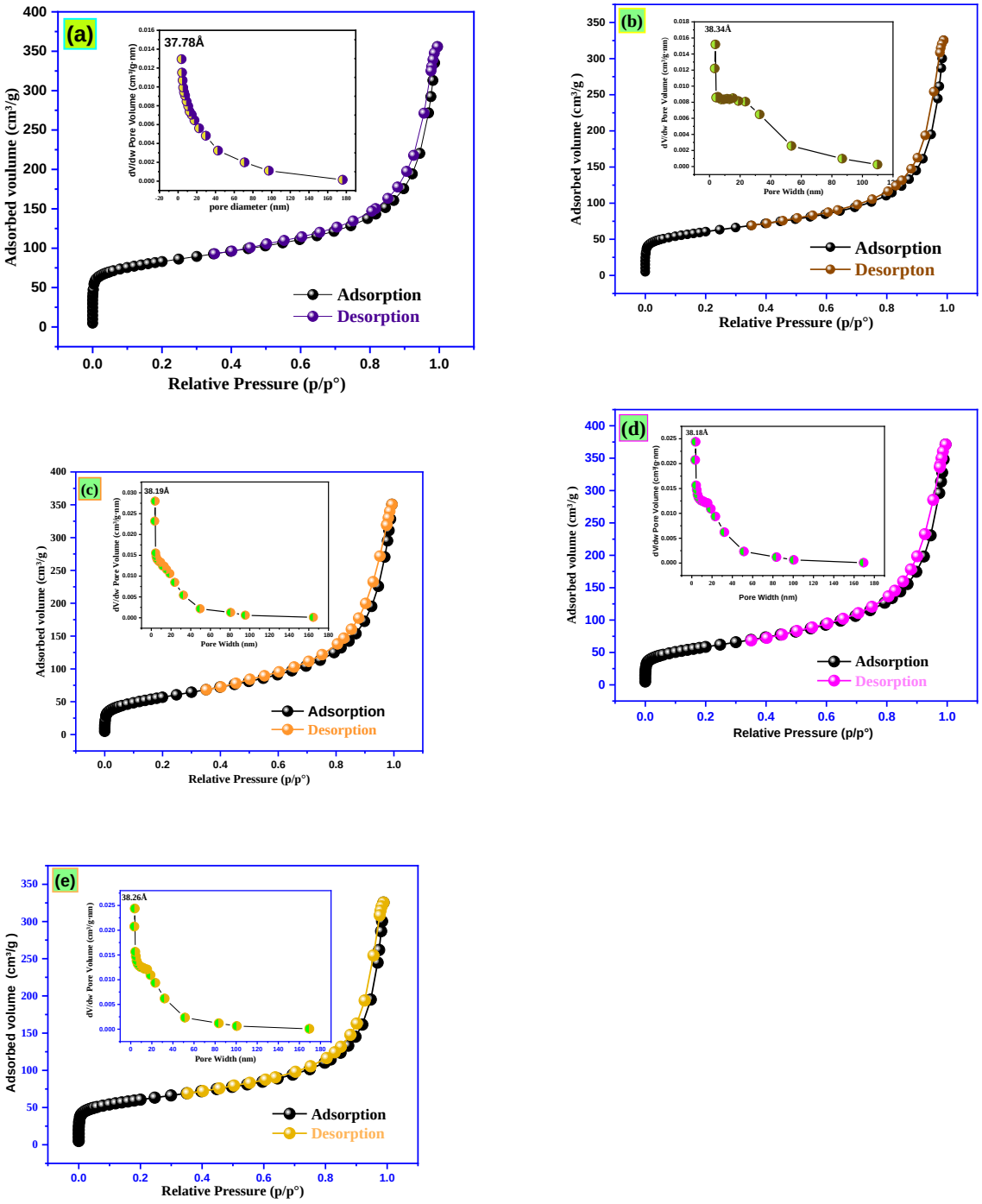

Fig.4. N_2 adsorption-desorption isotherms, and BJH pores, of the raw Sep (a), carbon@Sep 400 °C (b), carbon@Sep 450 °C (c), carbon@Sep 500 °C (d) and calcined raw Sep. 500 °C (e) adsorbents.

thermal treatment and the carbon modification of the sepiolite, significantly affect the specific surface area.

Table 3. Textural properties of raw Sep, Sep calcined at 500 °C, carbon@Sep 400 °C, carbon@Sep 450 °C and carbon@Sep 500 °C adsorbents.

Material	Surface area (m^2/g)	Pore volume (cm^3/g)	BJH adsorption average pore diameter (Å)
Raw Sep	**300.7**	**0.443**	**37.78 Å**
Raw Sep 500 °C	**216.6433**	**0.446**	**38.34 Å**
Carbon@Sep (400 °C)	**202.442**	**0.503**	**38.19 Å**
Carbon@Sep (450 °C)	**149.4804**	**0.371**	**38.18 Å**
Carbon@Sep (500 °C)	**207.5912**	**0.476**	**38.26 Å**

5.2. Effects of experimental conditions

5.2.1. Effect of the carbonization temperature

The influence of the carbonization temperature on the adsorption efficiency of the MG dye was studied by using 1g of the raw sepiolite sample which was added into 1 L of 100 mg/L MG solution at initial pH, for a contact time adsorbate-adsorbent of 4 h, resulting in MG-Sep hybrids (OSep). Thereafter, the MG-Sep powders were calcinated at temperatures ranging from 350 to 500 °C. Hence, as can be seen in Fig. 5, the MG adsorption on the calcined organo sepiolite was enhanced upon the organic sepiolite carbonization, and the adsorbed dye amount increased from 81 mg/g for Sep-350 °C at 99.5 mg/g Sep-500 °C, within an experimental error ranging from 2% to 4%. These results indicate that the adsorption of MG dye onto Carbon@Sep 500 °C is more efficient, in comparison to the raw sepiolite, Carbon@Sep 350 °C, Carbon@Sep 400 °C and the Carbon@Sep 450 °C. The

enhanced adsorption performance obtained by Carbon@Sep 500 can be explained by the high temperature effect which causes the sepiolite tunnel space increase and then facilitates the penetration of MG dye molecules inside the tunnels. In addition, the appearance of new COOH and OH adsorption sites may promote electrostatic interaction between the Carbon@Sep surface and the MG dye. Thus, all subsequent experiments in this work were performed using Carbon@Sep 500 °C

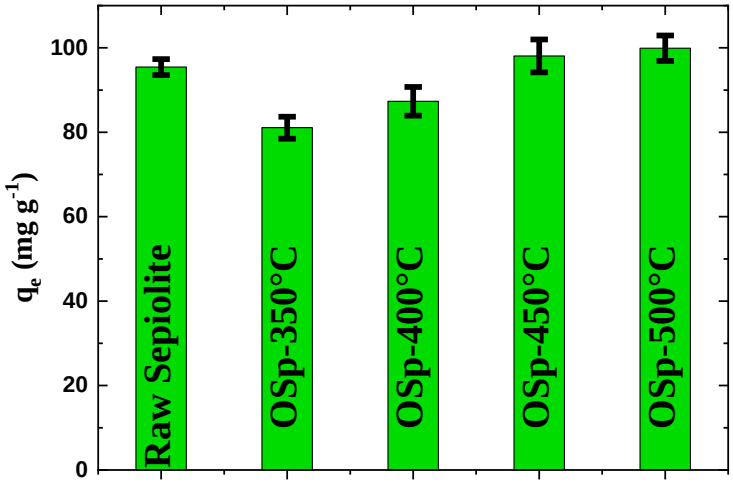

Fig. 5. Effect of carbonization temperature on the adsorption capacity of the raw and the organic sepiolite toward the MG dye (Adsorbent concentration=1 g/L, MG dye concentration=100 mg/L, initial pH, temperature = 25 °C).

5.2.2. Effect of the adsorbent dose on the MG dye adsorption

The effect of adsorbent dosage on the MG dye removal was investigated, at natural pH, by varying the Carbon (500°C) dose from 0.2 to 1.5 g. L^{-1}, and by fixing, the initial dye concentration to 100 mg L^{-1}, the contact time to 5 hours, and the adsorption temperature to 25°C. **Fig. 6** indicates that the MG removal efficiency is dependent on the Carbon@Sep dose in the aqueous solution. Thus, when the Carbon@Sep dose increases from 0.2 to 0.8 g/L, the

adsorbed MG amount, q_{ads}, decreases from 365 mg/g to 120 mg/g, within an experimental error ranging from 2% to 4%. Further, the MG removal increases from 73.2 to 96.1% and then reaches an almost constant value. The increase of removal rate can be due to the increase of the available active sites of the adsorbent, leading to enhancement in the contact surface area between the MG dye molecules and the adsorbent surface. Similar behavior has been reported in the literature [8, 11], for the MG removal by using other types of adsorbents.

In the following, an optimal Carbon@Sep dosage of 0.8 g L^{-1} will be used for further adsorption experiments.

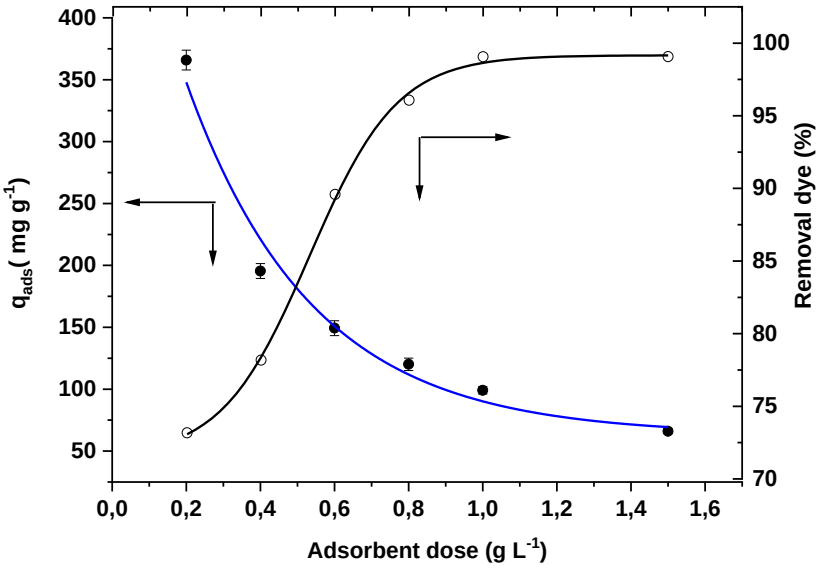

Fig.6. Effect of Carbon@Sep dosage on the MG adsorption (MG concentration=100 mg/L, contact time t=300 min, temperature T= 25 °C, adsorbent dosage = 0.2 g/L to 1.5 g/L, natural pH).

5.2.2. Effect of pH

The initial solution pH is an important parameter on the adsorption process [20, 21]. Thus, the adsorption of MG onto carbon@Sep was studied in the pH range of 2–12, by fixing, the initial dye concentration to 100 mg/L, the adsorbent dose to 0.8 g/L, and the contact time to 5h. Fig.

7 shows the initial solution pH effect on the MG adsorption from water onto Sep-Carbon surface. As can be seen in Fig. 7, the removal efficiency and the adsorption capacity, increase significantly from 97.7 to 124.9 mg/g when the pH increases from 2 to 6, and from 124.9 to 124.68 mg/g when the pH value varies from 6 to 12, within an experimental error ranging from 4% to 6%. Thus, in acidic medium (pH<4), the surface of Carbon@Sep was more protonated due to the presence of protons H^+ in solution, which promotes electrostatic repulsion between the cationic dye MG and the surface of the adsorbent and consequently the reduction in the adsorbed amount in an acid medium.

At pH > 4, the surface of Carbon@Sep becomes more and more negative by the effect of the deprotonation of the surface functional groups (Si-OH, Mg-OH, -COOH and -OH) which leads to an increase in the density of the negatively charged surface groups of the sepiolite which in turn result in an electrostatic attraction between the adsorbent and the positively charged molecules of the MG dye.

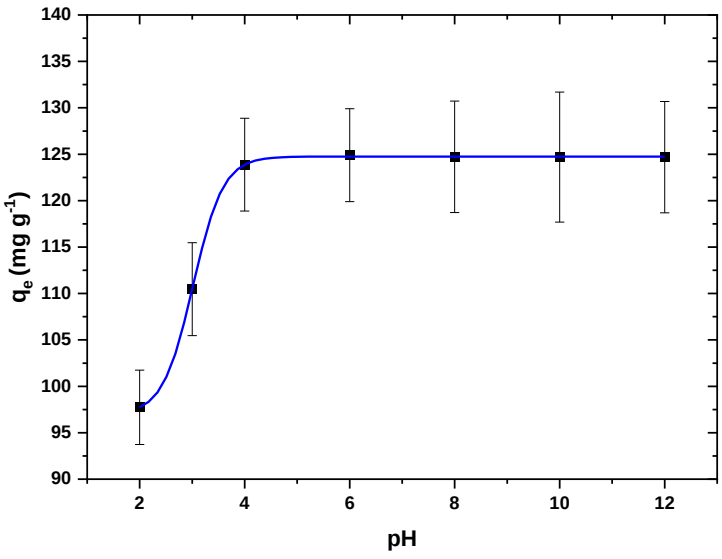

Fig. 7. MG removal effectiveness at different solution pH values using carbon@Sep (C_0=100 mg L^{-1}, adsorption time = 5 h, adsorbent dose = 0.8 g. L^{-1} and adsorption temperature, T= 25 °C)

According to these results, the electrostatic interactions between the MG dye and the Carbon@Sep surface play a predominant role in the adsorption phenomenon. Similar results were found by Haounati et al. (2020**)** in their reported work dealing with the adsorption of MG from water onto SDS/CTAB@Montmorillonite [21]. The optimal pH value of 6 was selected for next investigation since the maximum removal efficiency was attained at this pH.

5.2.4. Effect of the contact time

The contact time effect was examined for the MG adsorption onto Sep-Carbon, at 25°C, initial pH=6, 0.8 g/L of modified sepiolite dose and three MG concentrations (50, 100 and 150 mg/L). The obtained results are shown in Fig. 8. As seen in the figure, whatever is the dye concentration, the adsorption capacity of MG increases rapidly within the first 90 min, and then, slowly, until equilibrium point is reached at 300 min, within an experimental error ranging from 3% to 7%.. The first MG adsorption step can be explained by the high affinity of Sep-Carbon towards MG dye molecules.

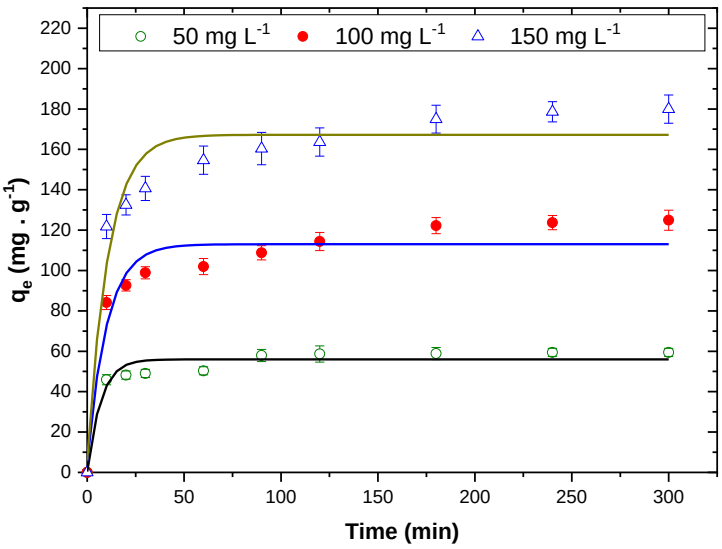

Fig.8. Effect of contact time and the MG concentration on the adsorption of MG dye onto Carbon@Sep (T= 25 °C, R= 0.8g/L, pH= 6)

The following slow step could be due to the penetration-diffusion of MG dye molecules into the inner surface of the modified sepiolite. Finally, after 300 min of contact time, all the active sites on the surface of the adsorbent are saturated and the adsorbed amount remains constant. Hence, the equilibrium time of 5h was fixed for all further adsorption experiments.

5.2.5. Adsorption kinetics

In order to describe the dye adsorption mechanism on the adsorbent surface, we carried out adsorption kinetics models. In addition, the experimental kinetics data were compared to the theoretical predictions of the pseudo first-order (PFO, Eq.3), pseudo second-order (PSO, Eq.4), and intraparticle diffusion (IPD) models (Eq. 5) [22]. The non-linear forms of PFO [23], [24], PSO [25-26] and IPD kinetic models are expressed in the following equations:

$$q_t = q_{e,1}(1-e^{-kl\,t}) \qquad \textbf{(Eq. 3)}$$

$$q_t = (q_e^2\, k_1 t)/(1+k_2 q_e t) \qquad \textbf{(Eq. 4)}$$

$$q_t = k_{IPD} t^{1/2} + \beta \qquad \textbf{(Eq. 5)}$$

where q_e(mg/g) and q_t(mg/g) are the amounts of adsorbed dye per weight of adsorbent (mg g^{-1}) at equilibrium and at time t(min), respectively; k_1 (min^{-1}), k_2 ($g.mg^{-1}.min^{-1}$) and k_{IPD} ($mg{\cdot}g^{-1}{\cdot}min^{1/2}$) are the rate constant of pseudo-first-order, pseudo-second-order and intraparticle diffusion adsorption, respectively. The non-linear plots of the pseudo-first-order and the pseudo-second-order models are presented in Fig. 9 (a). The parameters of kinetic models are calculated from the experimental data and are summarized, with correlation coefficients and χ values, in Table 4. As can be seen in this Table 4, and based on the higher correlation coefficient R^2 and lower χ values, the MG dye adsorption data were better fitted

by the pseudo-second-order (PSO) model for Sep/carbon. Furthermore, by using the PSO model, the calculated absorbed amounts $Q_{e.2}$ were better compared the experimental results ($Q_{e,\ exp}$), as depicted in Fig.9 (a). Therefore, the PSO model was found to be well suited to describe MG dye removal over Sep/carbon.

In addition, mass transfer mechanism of the slower adsorption phase between adsorbent/adsorbate was studied by using Intra-Particular-Diffusion model. Fig. 9 (b) displays the Q_t vs the time square root ($t^{1/2}$) plots for Sep-Carbon during MG dye adsorption. From Fig. 9 (b), the MG dye adsorption process presents a multi-linear profile, indicating that the adsorption process occurs through three successive steps [27]. The initial step describes the mobility of MG ions from liquid phase to the external surface of Sep-Carbon (surface diffusion), and the rate of this step is high. The second phase indicates the penetration of MG dye molecules into internal surface of modified sepiolite, and the rate of this step is lower than the first one and mainly controlled by pore diffusion. The third step is attributed to ultimate adsorption equilibrium. As can be seen in Fig. 9 (b), none of the lines passed through the origin, indicating that the intra-particle diffusion was not the only rate-controlling step [28-30], and others mechanisms such as boundary layer may control the adsorption process to some extent [31]. In this part dealing with intraparticle diffusion (IPD), the values of k_{IPD} and β, obtained from fitting the initial, second and third linear portions, to equation (5), are listed in Table 4. As can be observed in Table 4, increasing the initial MG concentration from 50 to 100 mg. L^{-1}, increases the values of β from 0.57 to 1.70, reflecting thus, the increase in the boundary layer thickness [32], and the probable decrease of the external mass transfer. Thus, the chance of internal mass transfer was increased [33].

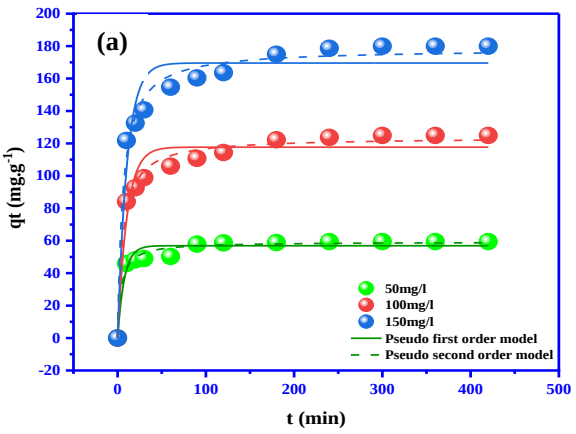

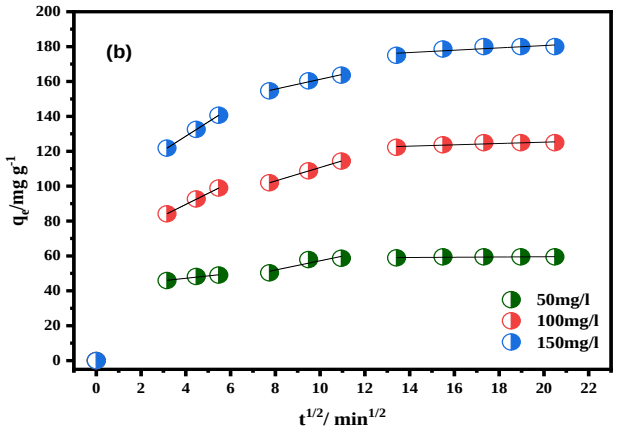

Fig.9. PFO, PSO (a) and IPD (b) correlation plots for MG dye adsorption onto the Sep-Carbon adsorbent.

5.2.6. Adsorption isotherm

The effect of initial MG concentration on its removal by Sep-Carbon was studied at different concentrations ranging from 25 to 1400 mg L^{-1} at 25°C and pH=6. As shown in Fig. 10, the adsorbed amounts of MG dye increases gradually with increasing its initial concentration. Hence, when the initial MG concentration increases from 10 to 1200 mg/L, the adsorbed amount of the dye increases several folds from 12.4 to 1188.82 mg/g. This behavior may be explained by the diffusion of the dye molecules from the solution toward the Sep-Carbon surface as caused by the increase of the driving force for mass transfer [34-35]. In order to elucidate the adsorption mechanism, the adsorption experimental data were compared to two theoretical models, the Langmuir model [36] and the Freundlich model [37].

The nonlinear equations of Langmuir (Eq.6) and Freundlich (Eq.7) models are given below:

$$Q_e = \frac{Q_m K_L C_e}{1 + K_L C_e} \qquad \textbf{(Eq. 6)}$$

$$Q_e = K_F C_e^{1/n} \qquad \textbf{(Eq. 7)}$$

where Q_e (mg/g) is the equilibrium adsorbed amount, Ce (mg/L) is the equilibrium concentration, Q_m (mg/g) is the maximum adsorbed amount, K_L(L/mg) and K_F (mg/g)/(mg/L)$^{1/n}$ are the Langmuir and Freundlich adsorption constants, respectively, n is the Freundlich isotherm exponent that determines the isotherm non-linearity. Hence, the adsorption is favorable for n>1 and unfavorable when 0<n<1.

Table 4. Kinetic parameters for the adsorption of MG onto Sep-Carbon.

	Pseudo–first-order (PFO)					Pseudo-second-order (PSO)			
C_0 (mg/l)	$Q_{e,exp}$ (mg g^{-1})	$Q_{e,1}$ (mg.g^{1})	k_1 (min^{-1})	R^2	χ	$Q_{e,2}$ (mg g^{-1})	k_2 (mg g^{-1}min^{1})	R^2	χ
50	59.4	56.9	0.133	0.95	4.03	59.29	0.0043	0.98	2.44
100	124.9	117.7	0.095	0.94	9.42	123.79	0.0013	0.98	5.37
150	179.9	169.6	0.094	0.94	12.56	178.30	0.0009	0.98	6.49

Intraparticle diffusion (IPD)

	Initial linear portion				Second linear portion				Third linear portion			
C_0	k_{IPD}	β	R^2	χ	k_{IPD}	β	R^2	χ	k_{IPD}	β	R^2	χ
50	54.2	0.57	0.99	0.15	99.5	7.33	0.89	2.19	61.8	0.66	0.84	0.19
100	128.9	1.70	0.99	0.97	161.5	4.50	0.99	0.49	134.0	1.39	0.99	0.07
150	176.9	1.45	0.98	1.42	190.5	1.79	0.99	0.18	200.1	1.90	0.97	0.58

Further, to assess the goodness of the fits, the correlation coefficients $R^{2,}$ and the χ values were determined and they are presented in Table 5. Recall that the Langmuir model considers that the adsorption takes place on a homogeneous surface leading to the formation of a monolayer of the adsorbate on the adsorbent surface. On the other hand, the Freundlich model assumes that the adsorption process takes place in more than one surface layer (multilayer) and that the adsorbent surface is heterogeneous, with a non-uniform distribution of heat of adsorption.

When the organic sepiolite was used as adsorbent, the fitting of the adsorption experimental data to the Langmuir model yielded higher R^2 coefficient (R^2=0.94) and lowest χ (χ=77.02) values, in comparison to the Freundlich model. This finding suggests that the MG dye adsorption forms a monolayer pattern on a homogeneous adsorbent surface, and a saturated adsorption capacity is expected due to limited adsorptive sites on the surface. The maximum dye adsorption capacity was determined to be 1198.67 mg g^{-1} on the organic sepiolite. Such high dye adsorbed amount value indicates that the organic sepiolite material can be used as potential adsorbent to efficiently clean-up the industrial effluent containing dyes.

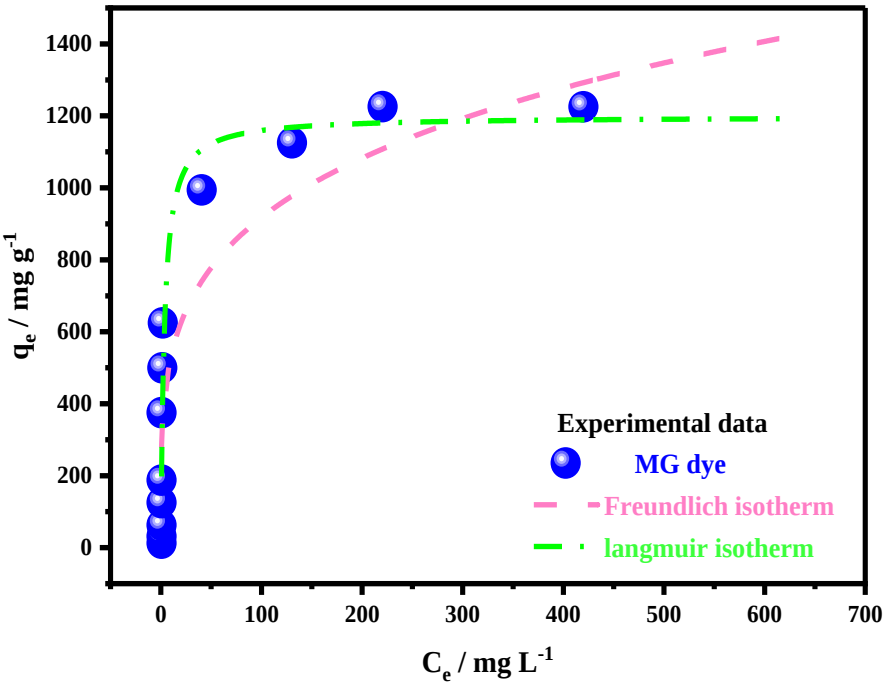

Fig. 10. Experimental adsorption isotherms of MG onto Sep-Carbon, compared to the nonlinear Langmuir and Freundlich theoretical models.

Table 5. Isotherms parameters for the MG adsorption from water onto the modified Sepiolite surface.

	Langmuir				Freundlich			
Dye	Q_m (mg/g)	K_L (L/mg)	R^2	χ	K_f (mg/g)	n	R^2	χ
MG	1198.67	0.2941	0.94	77.02	305.9	4.19	0.848	95.85

The comparison of the adsorption capacity of the sepiolite-carbon, used in the present work, with others adsorbents, as reported in the literature, for MG dye, is presented in Table 6. Clearly, our prepared adsorbent, as compared to different adsorbents reported in the literature, showed the highest MG adsorption capacity. This could be explained by the presence on the adsorbent surface of mineral functions such as Si-OH, Mg-OH and organic functions

carboxylic groups –COOH and hydroxyl groups -OH that are able to interact with the cationic MG dye through electrostatic interactions and hydrogen bonding, improving hence the MG removal from water.

Table 6. Comparison of the adsorption capacity of the modified sepiolite with other adsorbents reported in the literature, for the MG dye removal from water

Adsorbent	pH	t_c (min)	R (g/l)	T (°C)	Q_m ($mg.g^{-1}$)	References
Pine wood decayed by fungi Poria cocos	**4**	**1140** (24h)	**2**	**40**	**42.63**	[38]
Magnetic Nickel Oxide Nanoparticles	**7**	**40**	**-**	**25**	**87.72**	[39]
Rice husk	**6**	**60**	**-**	**40**	**7.40**	[40]
acid treated coffee husk	**6.8**	**120**	**0.2**	**60**	**263**	[41]
SDS/CTAB@Montmorillonite organoclay composites	**6**	**140**	**1**	**25**	**1021.45**	[25]
almond gum	**7**	**120**	**5**	**30**	**172.41**	[42]
diatomite	**7**	**90**	**-**	**25**	**23.64**	[28]
Chitosan/ sepiolite clay/ algae bio composite	**8**	**17,5**	**0,1**	**30**	**515,7**	[43]
Carbon@Sep	**6**	**240**	**0,8**	**25**	**1198.67**	**This study**

Thermodynamic analysis

To better understand the adsorption process, the determination of the MG dye adsorption thermodynamic parameters is important. Accordingly, the MG adsorption from aqueous solution onto organic Sep adsorbent was carried out in the temperature range varying from 298 to 338 K. The thermodynamic parameters such as ΔG°, ΔH° and ΔS° were then calculated according to the following equations:

$$\Delta G^{\circ} = -RT \ln K_e^{\circ} \qquad \textbf{(Eq. 8)}$$

$$\Delta G^{\circ} = \Delta H^{\circ} - T\Delta S^{\circ} \quad \textbf{(Eq. 9)}$$

$$\ln K_e^{\circ} = \frac{-\Delta H^{\circ}}{RT} + \frac{\Delta S^{\circ}}{R} \quad \textbf{(Eq. 10)}$$

$$K_e^{\circ} = \frac{(1000 \times K \times molecular \cdot weight \cdot of \cdot adsorbate) \times [adsorbate]^{\circ}}{\gamma}$$

Where: R is the universal gas constant (8.314 J $K^{-1}mol^{-1}$),

T is the absolute temperature (K),

K_e° is the thermodynamic equilibrium constant,

γ is the coefficient of activity (dimensionless),

[adsorbate]° is the standard concentration of the adsorbate (mol L^{-1}),

K_L (L/mg) is the Langmuir equilibrium constant.

Thus, as can be seen in Fig. 11 (a), the adsorption capacity of MG dye increases as the temperature value increases in the range of 298-338 °K. Thus, at higher temperature the maximum adsorbed amount of the MG dye is reached. Further, the plot of $\ln K_e^{\circ}$ versus 1/T is shown in Fig. 11 (b). The changes in entropy ΔS° and in enthalpy ΔH° were determined, respectively, from the intercept and the slope [44- 45] of the $\ln K_e^{\circ}$ versus 1/T curves. The obtained values of the thermodynamic parameters, of the MG dye adsorption on the Carbon@Sep, are presented in Table 7. The negative values of ΔG° indicate that the dye adsorption process over the temperature range of T=298-338K is spontaneous and feasible. It can also be observed that the ΔG° magnitude values increase from -27.82 to -34.46 $KJ.mol^{-1}$, with increasing temperature, indicating that the adsorption process was more favorable at higher temperatures in the studied range. In addition, the obtained positive value of ΔH° (26.8 kJ. mol^{-1}) indicates that the dye adsorption process is endothermic. Furthermore, when comparing the positive value of ΔH°, which is lower than 40 kJ mol^{-1}, to the ΔG° value which is approximately equal to -20kJ/mol, it is likely that the adsorbate-adsorbent interaction has a physisorption character [44]. Finally, the positive value of ΔS° indicates an increase in the system's randomness at the solid-solution interface during the adsorption of MG dye adsorption on the Carbon@Sep composite.

Table 7. Thermodynamic parameters for adsorption of MG dye onto Sep-Carbon composite.

T (K)	q_{ads} (mg/g)	K_L (L/mg)	Ke° *10^3	ΔG° (KJ.mol^{-1})	ΔH° (KJ.mol^{-1})	ΔS° (KJ.mol^{-1}.K^{-1})
298	1198.67	0.294	75.19	-27.82313	26.8	0.127
313	1225.5	0.307	112.17	-32.55455		
323	1241	0.454	165.67	-34.0727		
333	1248.3	0.698	254.68	-34.4686		

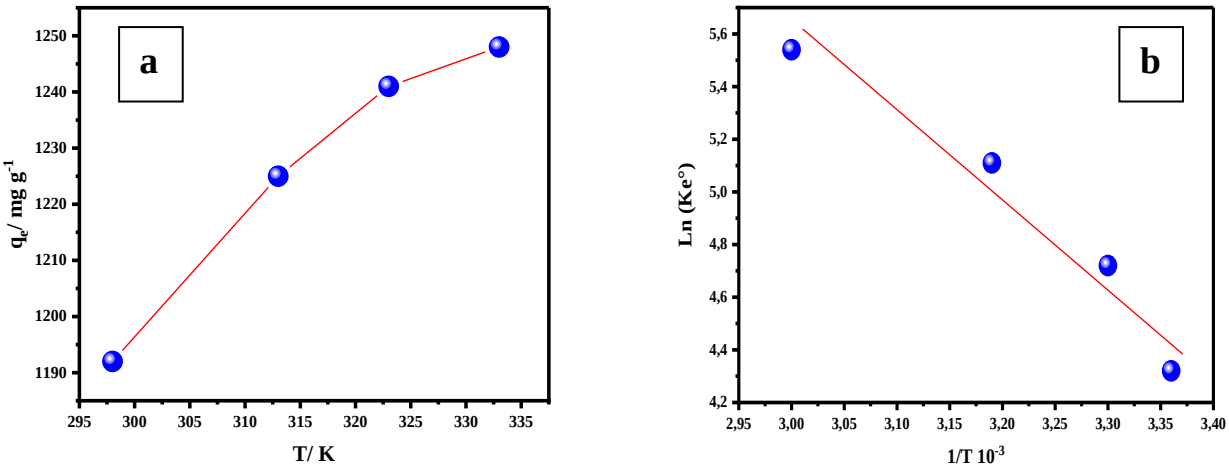

Fig. 11. (a) Effects of temperature on the adsorption of MG onto Sep-Carbon; (b) Van't Hoff plot of MG removal by Sep-Carbon composite.

6. Conclusions

In summary, Sepiolite-carbon composite adsorbents were prepared by adsorbing maximum amount of Malachite Green (MG) dye on the pristine sepiolite, followed by drying, and calcinating the resulting mixture at temperatures ranging from 350 to 500 °C for 3 h. The Sepiolite-carbon composite sample heated at 500°C (carbon@sepiolite, 500°C) was found to have the highest specific surface area (207,59 m^2/g), and showed the highest MG adsorption

capacity of 1198.67 mg/g at 25°C, when it was compared to others adsorbents cited the literature. Further, at the equilibrium, a good agreement was found between the experimental adsorption data and the theoretical Langmuir isotherm, whereas the kinetic adsorption isotherms were found to follow the pseudo-second-order model. The temperature effect on the MG removal from water onto carbon@sepiolite, 500°C, revealed that the adsorption process was spontaneous, endothermic and led to an increase in the randomness at the solid-solution interface. The overall data indicate that suitable adsorbents for the treatment of effluents containing cationic dyes can be designed by organically modified sepiolite. Carboxylic and hydroxylic functional groups, formed on the organically modified clay mineral surface, were found to be responsible for the efficient dye removal from water and the strengthen interaction occurring between the dye molecules and the adsorbent surface.

Acknowledgments

This work results from collaboration between Ibn Zohr University, Agadir – Morocco and the Institute of Materials Science of Mulhouse (IS2M), Haute Alsace University, Mulhouse - France. We thank VAULOT Cyril (IS2M), VIDAL Loïc (IS2M), and GREE Simon (IS2M) for the analyses of samples by, BET, SEM-TEM, and FTIR spectroscopy, respectively.

Data Availability. All data are included within the text.

Conflict of Interest. The authors declare no competing interests.

References

1. Alakhras, F., Alhajri, E., Haounati, R., Ouachtak, H., Addi, A.A., Saleh, T.A.: A comparative study of photocatalytic degradation of Rhodamine B using natural-based zeolite composites. Surfaces and Interfaces. 20, 100611 (2020). https://doi.org/10.1016/j.surfin.2020.100611

2. Haounati, R., Alakhras, F., Ouachtak, H., Saleh, T.A., Al-Mazaideh, G., Alhajri, E., Jada, A., Hafid, N., Addi, A.A.: Synthesized of Zeolite@Ag2O Nanocomposite as Superb Stability Photocatalysis Toward Hazardous Rhodamine B Dye from Water. Arab. J. Sci. Eng. (2022). https://doi.org/10.1007/s13369-022-06899-y

3. Haounati, R., El Guerdaoui, A., Ouachtak, H., El Haouti, R., Bouddouch, A., Hafid, N., Bakiz, B., Santos, D.M.F., Labd Taha, M., Jada, A., Ait Addi, A.: Design of direct Z-scheme superb magnetic nanocomposite photocatalyst Fe3O4/Ag3PO4@Sep for hazardous dye degradation. Sep. Purif. Technol. 277, 119399 (2021). https://doi.org/10.1016/j.seppur.2021.119399

4. Largo, F., Haounati, R., Akhouairi, S., Ouachtak, H., El Haouti, R., El Guerdaoui, A., Hafid, N., Santos, D.M.F., Akbal, F., Kuleyin, A., Jada, A., Addi, A.A.: Adsorptive removal of both cationic and anionic dyes by using sepiolite clay mineral as adsorbent: Experimental and molecular dynamic simulation studies. J. Mol. Liq. 318, (2020). https://doi.org/10.1016/j.molliq.2020.114247

5. Ouachtak, H., Akhouairi, S., Haounati, R., Addi, A.A., Jada, A., Taha, M.L., Douch, J.: 3,4-Dihydroxybenzoic acid removal from water by goethite modified natural sand column fixed-bed: experimental study and mathematical modeling. Desalin. WATER Treat. 194, 439–449 (2020). https://doi.org/10.5004/dwt.2020.25562

6. Regti, A., Lakbaibi, Z., Ben El Ayouchia, H., El Haddad, M., Laamari, M.R., El Himri, M., Haounati, R.: Hybrid Methods Combining Computational and Experimental Measurements for the Uptake of Eriochrome Black T Dye Utilising Fish Scales. Int. J. Environ. Anal. Chem. 1–20 (2021). https://doi.org/10.1080/03067319.2021.1929199

7. Akhouairi, S., Ouachtak, H., Addi, A.A., Jada, A., Douch, J.: Natural Sawdust as Adsorbent for the Eriochrome Black T Dye Removal from Aqueous Solution. Water,

524 Air, Soil Pollut. 230, 181 (2019). https://doi.org/10.1007/s11270-019-4234-6

525 8. Altinişik, A., Gür, E., Seki, Y.: A natural sorbent, Luffa cylindrica for the removal of a
526 model basic dye. J. Hazard. Mater. 179, 658–664 (2010).
527 https://doi.org/10.1016/j.jhazmat.2010.03.053

528 9. Daneshvar, N., Ayazloo, M., Khataee, A.R., Pourhassan, M.: Biological decolorization
529 of dye solution containing Malachite Green by microalgae Cosmarium sp. Bioresour.
530 Technol. 98, 1176–1182 (2007). https://doi.org/10.1016/j.biortech.2006.05.025

531 10. Oladipo, A.A., Ifebajo, A.O., Nisar, N., Ajayi, O.A.: High-performance magnetic
532 chicken bone-based biochar for efficient removal of rhodamine-B dye and tetracycline:
533 Competitive sorption analysis. Water Sci. Technol. 76, 373–385 (2017).
534 https://doi.org/10.2166/wst.2017.209

535 11. Oladipo, A.A., Gazi, M.: Uptake of Ni2+ and rhodamine B by nano-
536 hydroxyapatite/alginate composite beads: batch and continuous-flow systems. Toxicol.
537 Environ. Chem. 98, 189–203 (2016). https://doi.org/10.1080/02772248.2015.1115506

538 12. Oladipo, A.A., Gazi, M.: Enhanced removal of crystal violet by low cost alginate/acid
539 activated bentonite composite beads: Optimization and modelling using non-linear
540 regression technique. J. Water Process Eng. 2, 43–52 (2014).
541 https://doi.org/10.1016/j.jwpe.2014.04.007

542 13. Xie, W., Zhang, M., Liu, D., Lei, W., Sun, L., Wang, X.: Photocatalytic TiO 2 /porous
543 BNNSs composites for simultaneous LR2B and Cr (VI) removal in wool dyeing bath.
544 J. Photochem. Photobiol. A Chem. 333, 165–173 (2017).
545 https://doi.org/10.1016/j.jphotochem.2016.10.024

546 14. Narayani, H., Augustine, R., Sumi, S., Jose, M., Deepa Nair, K., Samsuddin, M.,

Prakash, H., Shukla, S.: Removal of basic and industrial azo reactive dyes from aqueous solutions via Fenton-like reactions using catalytic non-magnetic Pd-flyash and magnetic Pd-Fe3O4-flyash composite particles. Sep. Purif. Technol. 172, 338–349 (2017). https://doi.org/10.1016/j.seppur.2016.08.027

15. Martins, B.F., de Toledo, P.V.O., Petri, D.F.S.: Hydroxypropyl methylcellulose based aerogels: Synthesis, characterization and application as adsorbents for wastewater pollutants. Carbohydr. Polym. 155, 173–181 (2017). https://doi.org/10.1016/j.carbpol.2016.08.082

16. Praveen, S., Jegan, J., Bhagavathi, T., Ravindiran, P.: Biochar for removal of dyes in contaminated water : an overview. Biochar. 1–16 (2022). https://doi.org/10.1007/s42773-022-00131-8

17. Bulgariu, L., Escudero, L.B., Bello, O.S., Iqbal, M., Nisar, J., Adegoke, K.A., Alakhras, F., Kornaros, M., Anastopoulos, I.: The utilization of leaf-based adsorbents for dyes removal: A review. J. Mol. Liq. 276, 728–747 (2019). https://doi.org/10.1016/j.molliq.2018.12.001

18. El Haouti, R., Ouachtak, H., El Guerdaoui, A., Amedlous, A., Amaterz, E., Haounati, R., Addi, A.A., Akbal, F., El Alem, N., Taha, M.L.: Cationic dyes adsorption by Na-Montmorillonite Nano Clay: Experimental study combined with a theoretical investigation using DFT-based descriptors and molecular dynamics simulations. J. Mol. Liq. 290, 111139 (2019). https://doi.org/10.1016/j.molliq.2019.111139

19. Ouachtak, H., El Guerdaoui, A., Haounati, R., Akhouairi, S., El Haouti, R., Hafid, N., Ait Addi, A., Šljukić, B., Santos, D.M.F., Taha, M.L.: Highly efficient and fast batch adsorption of orange G dye from polluted water using superb organo-montmorillonite: Experimental study and molecular dynamics investigation. J. Mol. Liq. 335, 116560

(2021). https://doi.org/10.1016/j.molliq.2021.116560

20. de Souza, T.N.V., de Carvalho, S.M.L., Vieira, M.G.A., da Silva, M.G.C., Brasil, D. do S.B.: Adsorption of basic dyes onto activated carbon: Experimental and theoretical investigation of chemical reactivity of basic dyes using DFT-based descriptors. Appl. Surf. Sci. 448, 662–670 (2018). https://doi.org/10.1016/j.apsusc.2018.04.087

21. Haounati, R., Ouachtak, H., El Haouti, R., Akhouairi, S., Largo, F., Akbal, F., Benlhachemi, A., Jada, A., Addi, A.A.: Elaboration and properties of a new SDS/CTAB@Montmorillonite organoclay composite as a superb adsorbent for the removal of malachite green from aqueous solutions. Sep. Purif. Technol. 255, (2021). https://doi.org/10.1016/j.seppur.2020.117335

22. Yu, J., He, W., Liu, B.: Adsorption of acid orange II with two step modified sepiolite: Optimization, adsorption performance, kinetics, thermodynamics and regeneration. Int. J. Environ. Res. Public Health. 17, (2020). https://doi.org/10.3390/ijerph17051732

23. Boukoussa, B., Mokhtar, A., El Guerdaoui, A., Hachemaoui, M., Ouachtak, H., Abdelkrim, S., Addi, A.A., Babou, S., Boudina, B., Bengueddach, A., Hamacha, R.: Adsorption behavior of cationic dye on mesoporous silica SBA-15 carried by calcium alginate beads: Experimental and molecular dynamics study. J. Mol. Liq. 333, 115976 (2021). https://doi.org/10.1016/j.molliq.2021.115976

24. Ouachtak, H., Akhouairi, S., Ait Addi, A., Ait Akbour, R., Jada, A., Douch, J., Hamdani, M.: Mobility and retention of phenolic acids through a goethite-coated quartz sand column. Colloids Surfaces A Physicochem. Eng. Asp. 546, 9–19 (2018). https://doi.org/10.1016/j.colsurfa.2018.02.071

25. Haounati, R., Ouachtak, H., El Haouti, R., Akhouairi, S., Largo, F., Akbal, F.,

Benlhachemi, A., Jada, A., Addi, A.A.: Elaboration and properties of a new SDS/CTAB@Montmorillonite organoclay composite as a superb adsorbent for the removal of malachite green from aqueous solutions. Sep. Purif. Technol. 255, 117335 (2021). https://doi.org/10.1016/j.seppur.2020.117335

26. Gusmão, K.A.G., Gurgel, L.V.A., Melo, T.M.S., Gil, L.F.: Adsorption studies of methylene blue and gentian violet on sugarcane bagasse modified with EDTA dianhydride (EDTAD) in aqueous solutions: Kinetic and equilibrium aspects. J. Environ. Manage. 118, 135–143 (2013). https://doi.org/10.1016/j.jenvman.2013.01.017

27. Yuh-Shan, H.: Citation review of Lagergren kinetic rate equation on adsorption reactions. Scientometrics. 59, 171–177 (2004). https://doi.org/10.1023/B:SCIE.0000013305.99473.cf

28. Tian, L., Zhang, J., Shi, H., Li, N., Ping, Q.: Adsorption of Malachite Green by Diatomite: Equilibrium Isotherms and Kinetic Studies. J. Dispers. Sci. Technol. 37, 1059–1066 (2016). https://doi.org/10.1080/01932691.2015.1080610

29. Tran, H.N., You, S.-J., Hosseini-Bandegharaei, A., Chao, H.-P.: Mistakes and inconsistencies regarding adsorption of contaminants from aqueous solutions: A critical review. Water Res. 120, 88–116 (2017). https://doi.org/10.1016/j.watres.2017.04.014

30. Ho, Y.S., McKay, G.: Comparative sorption kinetic studies of dye and aromatic compounds onto fly ash. J. Environ. Sci. Heal. Part A. 34, 1179–1204 (1999). https://doi.org/10.1080/10934529909376889

31. Blanchard, G., Maunaye, M., Martin, G.: Removal of heavy metals from waters by means of natural zeolites. Water Res. 18, 1501–1507 (1984). https://doi.org/10.1016/0043-1354(84)90124-6

32. Tang, D., Zhang, G.: Efficient removal of fluoride by hierarchical Ce-Fe bimetal oxides adsorbent: Thermodynamics, kinetics and mechanism. Chem. Eng. J. (2016). https://doi.org/10.1016/j.cej.2015.08.019

33. Akbar, M., Irohara, T.: Scheduling for sustainable manufacturing: A review. J. Clean. Prod. 205, 866–883 (2018). https://doi.org/10.1016/j.jclepro.2018.09.100

34. Marrakchi, F., Khanday, W.A., Asif, M., Hameed, B.H.: Cross-linked chitosan/sepiolite composite for the adsorption of methylene blue and reactive orange 16. Int. J. Biol. Macromol. 93, 1231–1239 (2016). https://doi.org/10.1016/j.ijbiomac.2016.09.069

35. Langmuir, I.: THE ADSORPTION OF GASES ON PLANE SURFACES OF GLASS, MICA AND PLATINUM. J. Am. Chem. Soc. 40, 1361–1403 (1918). https://doi.org/10.1021/ja02242a004

36. Freundlich, H.: Über die Adsorption in Lösungen. Zeitschrift für Phys. Chemie. 57U, 385–470 (1907). https://doi.org/10.1515/zpch-1907-5723

37. Zhang, H., Tang, Y., Liu, X., Ke, Z., Su, X., Cai, D., Wang, X., Liu, Y., Huang, Q., Yu, Z.: Improved adsorptive capacity of pine wood decayed by fungi Poria cocos for removal of malachite green from aqueous solutions. Desalination. 274, 97–104 (2011). https://doi.org/10.1016/j.desal.2011.01.077

38. Mohanta, J., Dey, B., Dey, S.: Sucrose-Triggered, Self-Sustained Combustive Synthesis of Magnetic Nickel Oxide Nanoparticles and Efficient Removal of Malachite Green from Water. ACS Omega. (2020). https://doi.org/10.1021/acsomega.0c00999

39. Chowdhury, S., Mishra, R., Saha, P., Kushwaha, P.: Adsorption thermodynamics, kinetics and isosteric heat of adsorption of malachite green onto chemically modified

rice husk. Desalination. 265, 159–168 (2011).
https://doi.org/10.1016/j.desal.2010.07.047

40. Krishna Murthy, T.P., Gowrishankar, B.S., Chandra Prabha, M.N., Kruthi, M., Hari Krishna, R.: Studies on batch adsorptive removal of malachite green from synthetic wastewater using acid treated coffee husk: Equilibrium, kinetics and thermodynamic studies. Microchem. J. 146, 192–201 (2019).
https://doi.org/10.1016/j.microc.2018.12.067

41. Bouaziz, F., Koubaa, M., Kallel, F., Ghorbel, R.E., Chaabouni, S.E.: Adsorptive removal of malachite green from aqueous solutions by almond gum: Kinetic study and equilibrium isotherms. Int. J. Biol. Macromol. 105, 56–65 (2017).
https://doi.org/10.1016/j.ijbiomac.2017.06.106

42. Lima, E.C., Hosseini-Bandegharaei, A., Anastopoulos, I.: Response to “Some remarks on a critical review of the estimation of the thermodynamic parameters on adsorption equilibria. Wrong use of equilibrium constant in the van’t Hoff equation for calculation of thermodynamic parameters of adsorption - Journal of . J. Mol. Liq. (2019).
https://doi.org/10.1016/j.molliq.2019.01.160

43. Ren, S., Deng, J., Meng, Z., Wang, T., Xie, T., Xu, S.: Enhanced removal of phenol by novel magnetic bentonite composites modified with amphoteric-cationic surfactants. Powder Technol. (2019). https://doi.org/10.1016/j.powtec.2019.08.024

44. Atkin, P.W.: Physical chemistry, 4th edition. Oxford University Press, London, 1990